

Roll-steering for improving SAOCOM-SAR performances

D. Giudici¹, L. Maggi¹, A. Monti Guarnieri² *member, IEEE*, J. Medina³, M Völker⁴

¹ARESYS srl, Piazza Leonardo da Vinci, 32, 20133 Milano, Italy

² Politecnico di Milano, DEI, Piazza Leonardo da Vinci, 32, 20133 Milano, Italy

³CONAE Av Paseo Colón, 751, 1063 Buenos Aires, Argentina

⁴EADS Astrium - Astrium GmbH - D-88039 Friedrichshafen

phone: + 0039 0223993446, fax: +0039 0223993413, email: monti@elet.polimi.it

Abstract—In the design of a spaceborne Synthetic Aperture RADAR mission with multiple modes and swaths, like the forecoming Argentinean constellation SAOCOM, the minimization of the number of beams, Pulse Repetition Frequency (PRF) switching, and the optimization of the coverage are fundamental issues. The paper discusses the impact of the roll-steering maneuver on these issues. The optimization of roll-steering with respect to satellite altitude is found by a theoretical analysis on a simplified geometry, and by a numerical approach that accounts for the ellipsoidal earth and all the modes foreseen for the sensor. The solution found for the SAOCOM case, shows that a single set of beams and PRFs can be exploited for all the modes.

Index Terms— Synthetic Aperture Radar, STRIPMAP, TOPSAR. Conference topic: SAR/ISAR

I. INTRODUCTION

The future Argentinean constellation of two identical L-band SAOCOM satellites will have as strategic goals the mapping of soil moisture of the “Pampa humeda”, a 700 000 km² land dedicated to agriculture and cattle raising, and at the same time in cooperating with the Italian X-band COSMO constellation in the management of the emergency [1]. Such systems foreseen three acquisition modes each of them with two different polarization schemes: “Dual”, DP, (HH,HV or VV,VH) and “Quad” (full polarimetric), QP, with experimental circular polarization [2]. A very wide swath of about 300 km is achieved by exploiting TOPSAR scanning [3][4]. A summary of the performances in each mode is in Tab. I. If we combine the three modes, the two polarizations and the different incidence angles, we have a total of 24 different configurations, a few more should be added for getting the full compatibility with COSMO mission.

The design of such multi-mode systems must aim, as major goal, to the maximization of the coverage, and the minimization of the number of beams and PRF switching. The ground coverage in fact impact on the repeat pass, whereas the number of beams and PRF switching as a direct impact on the

calibration and the processing.

In order to understand how these goals are interdependent, let us revise the timing constraints in the design of a spaceborne SAR. Let us refer to the geometry of Fig. 1.a,

TABLE I
SAOCOM MODES

Mode	Polar.	Incidence angle deg	Swath depth ground (km)	Azimuth Resolution (m)
STRIP-MAP	Dual	20-50	30-50	5
	Quad	17-35	20-40	6
TOPSAR NARROW	Dual	25-48	150-170	30
	Quad	17-35	110	50
TOPSAR WIDE	Dual	25-48	350	50
	Quad	17-35	220	100

where we assumed for simplicity flat earth. The geometry draws the SAR antenna in the plane orthogonal to the trajectory, by assuming a sensor height H and a single swath included in the slant range intervals $R_m \leq R \leq R_M$. In the figure, we have defined with θ the look angle and P_N the location of the sensor’s Nadir.

Given this geometry, the timing of the on-board radar is constrained to avoid occurrence of the return echo during the transmission and during the return from Nadir [5]. The two-way return time from Nadir and echo of a target at distance R can be expressed as follows:

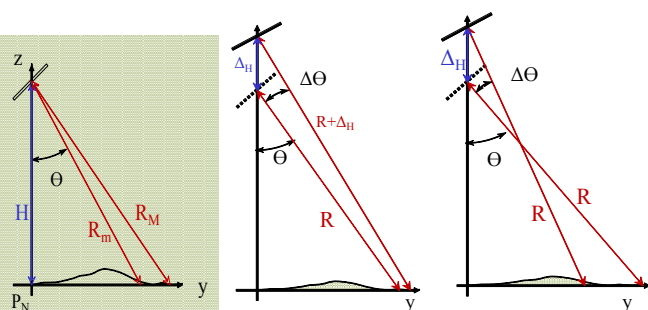


Fig. 1. Left: simplified SAR geometry, with flat earth. Center and right: required antenna rotation for compensating the Nadir and the echo return time at a different satellite height.

$$t_e = \frac{2R(\tau_k)}{c} \approx \frac{2}{c} \frac{H}{\cos \theta} \text{ where } \tau_k = \frac{k}{PRF} + \tau_0 \quad (1)$$

$$t_n \approx \frac{2H}{c}$$

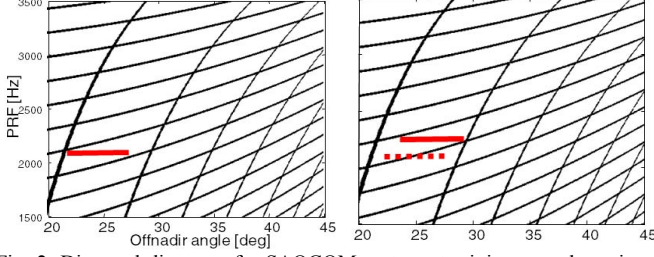


Fig. 2. Diamond diagrams for SAOCOM system at minimum and maximum satellite heights. In each diagram the dark bands corresponds to contributions of Nadir returns and transmit time, during which echoes cannot be received. The red line marks a possible beam / swath in both cases.

t_e , t_n being the echo and Nadir delays and τ_k the slow time of the transmission.

In (1) we have ignored the variation in delay due to the displacement of the platform along azimuth in the time corresponding to the two-way travel path and up to a few echoes afterwards.

The most used tool to design beams is the diamond diagram [5], as shown in Fig. 2, where the black stripes marks the combinations of PRF and off-nadir angle (hence range), that corresponds to Nadir return and to the transmission time. The thickness of the stripes has been assumed of 5 degrees for the Nadir return, and by accounting for a duty cycle of 5% for the transmission. In the diagram on the left, the possible angular interval for one beam is represented by the horizontal red line. The same range of angle is not allowed at a different height, the dotted line in the right diagram. However, we need to change both the range of angles, hence the beam, and the PRF, see the continuous line in the figure on the right.

This solution, that leads to a switch of PRF along the orbit and eventually a design of a new beam, has been so far adopted so in the majority of the spaceborne systems.

II. ROLL STEERING MANOUVER

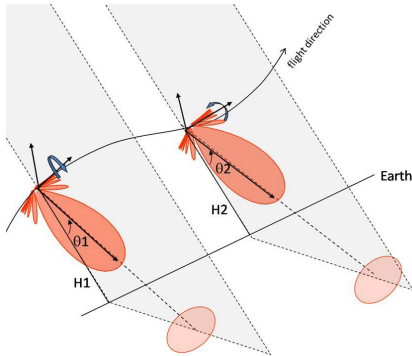


Fig. 3. Pictorial representation of the roll steering maneuver: the off-nadir angle is changed along track by a mechanical roll of the platform.

The roll steering maneuver was first introduced for ESA Sentinel-1SAR to minimize the switching of PRF along orbit (a major mission requirement) [6][7]. The principle is represented in Fig. 3, where a mechanical rotation of the platform result in rotating the whole antenna beam, and

pointing in a different range to compensate the effect of elevation changes.

For better understanding this compensation, let us refer to the two leftmost geometries in Fig 1. An increment of elevation Δ_H causes a proportional *shift of the Nadir return*. We are not able to compensate it with roll steering, however, we won't need that compensation if we shift the echo return of the same amount. If we define $r_e(\theta, H)$ the slant range of the target at a look angle θ and seen by an elevation H , we have to impose that at the new elevation, the look angle is modified to shift the range by the same amount of Nadir shift, that is Δ_H . The constraint that follows:

$$r_e(\theta + \Delta_\theta, H + \Delta_H) - r_e(\theta, H) = \Delta_H \quad (2)$$

can be solved by differentiating (1):

$$\frac{\partial r_e}{\partial H} \Delta_H + \frac{\partial r_e}{\partial \theta} \Delta_\theta = \Delta_H \Rightarrow \Delta_\theta = \frac{\cos \theta - 1}{H \tan \theta} \Delta_H \quad (3)$$

Δ_θ is the amount of look angle rotation, hence of roll steering, that would perfectly compensate the shift in Nadir echoes. Notice that it is θ -dependent, so it would be impossible to compensate simultaneously for all the swaths, and some error would be introduced.

We then need to impose the further constraint: that the return does not superpose with the echo transmission. As the latter is independent on the altitude the constraint should impose the same range (see Fig. 1 on the left):

$$\Delta r_e = \frac{c \Delta t_e}{2} = \frac{H}{\cos \theta} - \frac{H + \Delta_H}{\cos(\theta + \Delta_\theta)} = 0 \quad (4)$$

And it can be likewise can be solved by differentiating:

$$\frac{\partial r_e}{\partial H} = \frac{\partial r_e}{\partial \theta} \Rightarrow \Delta_\theta = \frac{1}{H \tan \theta} \Delta_H \quad (5)$$

We notice a similar dependence on the look angle as in (2). We should then find $\Delta_\theta(\Delta_H)$ to satisfy both constraints (3) and (5). This would then be integrated to get the perfect roll steering law, $\theta(\Delta_H)$. Unfortunately it is not possible to derive this solution, as the two constraints leads to two different surfaces, as Fig. 4 shows. Therefore, we need to minimize the error in some norm.

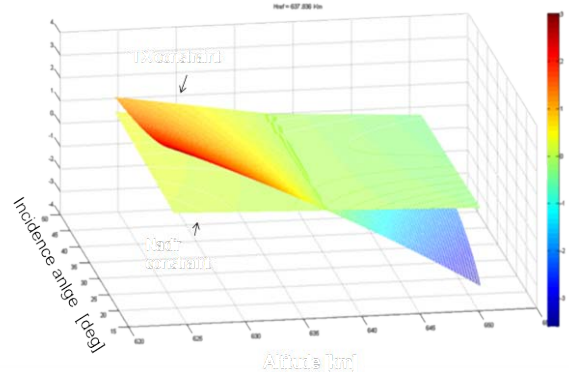


Fig. 4. The two surfaces shown would provide the differential roll that solve the two constraints involved in the roll steering determination.

III. ROLL STEERING OPTIMIZATION

In the design of the actual roll steering, we have to account that the optimization should apply to all the modes foreseen for the mission, hence for beams extending over a range of angles from 20° to 50° off-nadir angles, and for PRF from 1.7 to 4 kHz, including DP and QP modes. The difference is significant, the roll rate predicted by (5) would change from 0.07 deg/km ($\theta = 50^\circ$) to 0.23 deg/km ($\theta = 20^\circ$).

Furthermore, we need to account for ellipsoidal earth, instead than the flat one so far assumed.

Therefore, the optimization has been run by a numerical approach, in which the differential roll Δ_θ for each altitude Δ_H (with respect to a reference H_r) has been found by minimizing the following figure of merit:

$$W(\Delta_H) = \frac{\sum_k C(\Delta_H, PRF_k)}{\max\left(\sum_k C(\Delta_H, PRF_k)\right)} \quad (6)$$

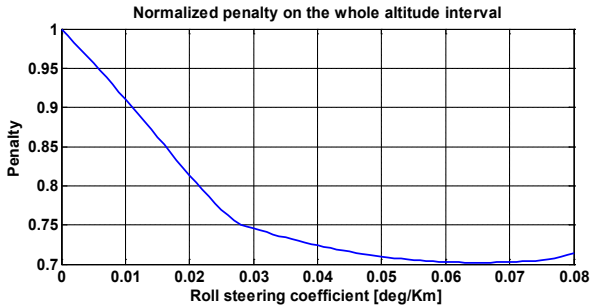
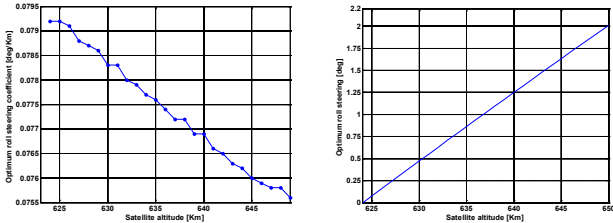
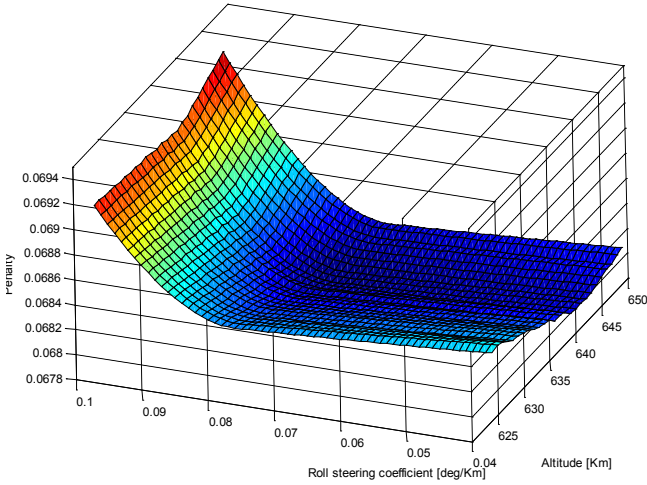


Fig. 5. Up surface: cost function used for optimizing the roll steering. Mid-right plot: optimal differential roll-steering as a function of satellite height. Mid-left plot: integration of the differential roll steering: notice that the curve is very close to linear. Lower plot: normalized cost as function of the linear roll steering rate.

where the summation is extended to all the PRFs in the diamond, and $C(\cdot)$ is the extent on the ground of the forbidden location, e.g. the shaded area in the diamonds. This cost function (penalty), is represented in the surface in Fig. 5, for each altitude, and for each differential roll steering. The optimum differential roll steering is plotted in the same figure together with the optimum roll steering, obtained by integrating the differential relation. We notice that the roll steering is very close to linear with height, as it came out from (3) and (5), therefore we found the linear rate that minimize the cost function, according to the last plot in Fig. 5. Notice that, at the optimal rate, the cost function improves of 70% with respect to the no-roll steering case.

Notice that the law is approximately linear with the elevation, as it could be derived also by looking at the constraints (3) and (5). To better explain the role of the roll steering, we have represented in Fig. 6 on the left the superposition of all the diamond diagram at different elevations. This what we would get without any roll. The amount of free-space available is so shrunk that there is no solution that conserves the PRFs and the beams. In the same figure, on the right, we have superposed all the diamond diagrams, after compensating each one by the optimal roll found here. The amount of free space is much more increased, allowing now for a single design over the whole orbit.

IV. SENSITIVITY ANALYSIS

In order to appreciate this fact, we can do a sensitivity on the simple geometry assumed in Fig. 1. The coverage on the ground can be approximated as:

$$C_g = \frac{C_s}{\sin \theta} = \frac{R_M - R_m}{\sin \theta}$$

Where C_s is the slant range coverage. Now we assume that the echo return time changes one of the two extremes, then the ground coverage variation is:

$$\Delta C_g = \frac{\partial r_e}{\partial H} \frac{1}{\sin \theta} \Delta_H = \frac{2}{\sin 2\theta} \Delta_H \quad (7)$$

This means that at off-nadir angle 30° we get 60 km change in the 25 km altitude variation of SAOCOM. AS the average SAOCOM swath is 50 km wide, the complete blocking of the diamond in Fig. 6 is justified. Moreover, if we consider the effect on Nadir return on slant range, we get:

$$\Delta C_g = \frac{\partial r_n}{\partial H} \frac{1}{\sin \theta} \Delta_H = \frac{1}{\sin \theta} \Delta_H \quad (8)$$

that compares closely to the condition (7).

V. SAOCOM MODE DESIGN

The superposition of diagrams after roll steering optimization in Fig. 6 has been assumed as the basis for the design of the beams and the PRF in the SAOCOM SAR. The actual design is shown in the diamond diagrams of Fig. 5. The design has been made following the guidelines for TOPSAR design and optimization in the paper [4]. The design basis on two sets, each of nine beams, one for DP (the left diagram in Fig. 5), and the other for QP (the right diagram in the same

figure).

These beams allows a continuous coverage through the whole orbit, with no PRF switch. Each beam corresponds to one STRIPMAP mode, whereas the medium resolution “TOPSAR NARROW” has been designed by combining three STRIPMAP beams in DP or five beams in QP, and the coarse resolution, “TOPSAR WIDE” (350 km coverage in DP and 250 in QP) combines 6 beams in DP and all the 9 QP beams.

VI. CONCLUSION

The feasibility of roll steering mode has been analyzed by both a theoretical approach based on a simplified geometry and a numerical approach suited for the actual beams design. This second approach led to the optimal roll steering, derived for each satellite altitude. The law is indeed very close to a smooth linear rate of 0.07 deg/km.

The use of roll steering has been shown quite effective for systems with small swaths, like for the L-band SAR or high resolution systems, allowing for a single set of beams and PRF can be kept though the whole orbit.

REFERENCES

- [1] F. Caltagirone, "Status, results and perspectives of the Italian Earth Observation SAR COSMO - SkyMed," Radar Conference, 2009. EuRAD 2009. European, vol., no., pp.330-334, Sept. 30 2009-Oct. 2 2009
- [2] D'Aria, D.; Giudici, D.; Guarnieri, A.M.; Rizzoli, P.; Medina, J., "A wide swath, full polarimetric, L band spaceborne SAR," Radar Conference, 2008. RADAR '08. IEEE, vol., no., pp.1-4, 26-30 May 2008
- [3] U Stein, M Younis, "Suppression of range ambiguities in synthetic aperture radar systems," proc EUROCON 2003, Vol 2, pp 417- 421
- [4] A. Monti Guarnieri, F. De Zan, " TOPSAR: Terrain Observation by Progressive Scans", in IEEE Trans. GRS, Vol 44, No. 9, pp 2352-2360, Sept. 2006. DOI: 10.1109/TGRS.2006.873853.
- [4] D. D'Aria, D. Giudici, F. De Zan, A. Monti Guarnieri, F. Rocca, "Burst mode SARs for wide swath surveys" in Canadian Journal of Remote Sensing, Vol. 33, No 1, pp 27-38, 2007
- [5] Baker, K.R.; Brown, A.D.; Currie, A.J., "Optimisation efficiency in behavioural synthesis," Circuits, Devices and Systems, IEE Proceedings -, vol.141, no.5, pp.399-406, Oct 1994
- [6] E. Attema, P. Snoeij, B. Duesmann, M. Davidson, N. Floury, B. Rosich, B. Rommen and G. Levrini, GMES SENTINEL-1 Mission and System, in Proc. of '4th Int. Workshop on Science and Applications of SAR Polarimetry and Polarimetric Interferometry – PolInSAR 2009', 26–30 January 2009, Frascati, Italy (ESA SP-668, April 2009)
- [7] German Patent Application 102008026497.0-55 "Verfahren zum Optimieren des Betriebs eines aktiven Seitensichtensensors bei veränderlicher Höhe über der zu erfassenden Oberfläche", June 2008.
- [8] US-Patent Application No. 12/476,904 "Method for optimizing the operation of an active lateral-view sensor when the height above the surface to be detected is variable", June 02, 2009.

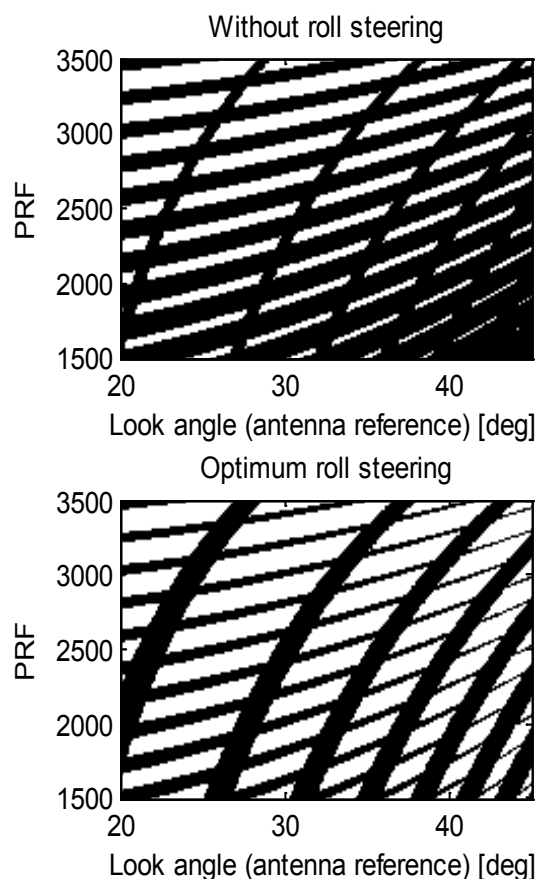


Fig. 6. Above: superposition of all the diamond diagrams made at different satellite altitude. Below: the same superposition in the case of optimal roll-steering.